

Cluster synchronization of spiking induced by noise and interaction delays in homogenous neuronal ensembles

Igor Franović,¹ Kristina Todorović,² Nebojša Vasović,³ and Nikola Burić^{4,a)}

¹Faculty of Physics, University of Belgrade, P.O. Box 44, 11001 Belgrade, Serbia

²Department of Physics and Mathematics, Faculty of Pharmacy, University of Belgrade, Vojvode Stepe 450, Belgrade, Serbia

³Department of Applied Mathematics, Faculty of Mining and Geology, University of Belgrade, PO Box 162, Belgrade, Serbia

⁴Scientific Computing Lab., Institute of Physics, University of Beograd, PO Box 68, 11080 Beograd-Zemun, Serbia

(Received 10 March 2012; accepted 4 September 2012; published online 19 September 2012)

Properties of spontaneously formed clusters of synchronous dynamics in a structureless network of noisy excitable neurons connected via delayed diffusive couplings are studied in detail. Several tools have been applied to characterize the synchronization clusters and to study their dependence on the neuronal and the synaptic parameters. Qualitative explanation of the cluster formation is discussed. The interplay between the noise, the interaction time-delay and the excitable character of the neuronal dynamics is shown to be necessary and sufficient for the occurrence of the synchronization clusters. We have found the two-cluster partitions where neurons are firmly bound to their subsets, as well as the three-cluster ones, which are dynamical by nature. The former turn out to be stable under small disparity of the intrinsic neuronal parameters and the heterogeneity in the synaptic connectivity patterns. © 2012 American Institute of Physics. [<http://dx.doi.org/10.1063/1.4753919>]

Synchronization of neuronal activity is considered as a fundamental dynamical ingredient of various brain functions. Therefore, multifarious properties of the synchronization dynamics in neural network models have been the topic of intensive and thorough research. Dynamics of realistic neuronal networks is crucially influenced by the interaction involving synaptic delays, and by small perturbations of various origin, which are commonly treated as noise. The impacts that noise or the interaction delays make on the dynamical properties of neuronal populations are diverse and well known. However, the systematic exploration of the co-effects introduced by the simultaneous presence of noise and time delay has begun only quite recently. An interesting type of the ensuing synchronization phenomena may be the splitting of a population into clusters, each made up of neurons oscillating in synchrony, whereby the activity between the clusters shows phase lags. Usually, the synchronization cluster formation is a consequence of some structural inhomogeneity, either in the local neuronal parameters or the network topology. In a recent letter, we briefly reported on the occurrence of synchronization clusters observed in a homogeneous network of excitable stochastic neurons with delayed coupling. Despite the network being completely structureless, the interplay of noise, time-delay and the excitable character of the neurons is found sufficient to trigger the clustering. This paper provides a thorough and systematic exploration of such spontaneous cluster formation.

brain, as it is associated with many cognitive processes,^{1–5} while also being crucial for movement preparation and execution.^{6–9} It is commonly believed that synchronously oscillating neurons exchange information more effectively.¹⁰ Neurons *in vivo* operate under the influence of many factors that can be modeled as noisy perturbation. Nontrivial and constructive role of noise in the dynamics of a single neuron, few neurons, or large neuronal networks is well known.^{11–19} The key to this lies in the fact that the excitable dynamics of a single neuron acts as an amplifier of the small noisy perturbation. The latter can shift a neuron near the stable fixed point of the excitable regime randomly into a state that yields a spike discharge. Such noise induced spiking resembles chaotic oscillations. However, for a certain range of noise intensity, which depends on the neuronal refractory period, spiking may appear as regular oscillation with a well defined frequency. Coupling to other neurons can then lead to synchronization between stochastic spiking or may induce deterministic oscillatory dynamics.

Transmission of neuronal impulses through an axon and synapses is not instantaneous. The transport time can be included phenomenologically into the modeling by using explicit time lag in the synaptic interaction terms. Relatively small interaction time delays are known to have profound effects on the neuronal dynamics.^{20–27} The time delay may induce oscillations through different mechanisms, such as the Hopf or some global bifurcations, or it may suppress the existing oscillations. It is also widely recognized how time delay can profoundly influence the type of synchronization between the neurons.

The effects of the simultaneous influence of noise and the interaction delays on the dynamics of typical neuronal systems have been analyzed much less, viz.,^{22,28} and the references therein. One such phenomenon, induced by combining the noise, interaction-delay and the excitable

I. INTRODUCTION

Selective synchronization of relevant neural populations is a general principle for organizing communication in the

^{a)}Electronic mail: buric@ipb.ac.rs.

character of the local dynamics, constitutes the splitting of population into clusters, each made up of synchronously firing neurons. So far, the issues gaining significant attention have been the formation of clusters of synchronous dynamics either due to the inhomogeneous distributions of the neuronal parameters or the non-trivial network topologies, see Refs. 10 and 29. Appreciating such studies, one would imagine the clusters emerging in structureless networks less likely. Note that this does not connote to systems of globally coupled identical oscillators, where clustering already constitutes a well-known manifestation of multistability, usually being associated with more complex interaction functions.^{30–32} However, it has recently been reported³³ that the synchronization clusters can be formed even in completely homogeneous networks of excitable units owing solely to a subtle interplay of noise, interaction delay and the neuronal excitability. In this paper, we provide an in-depth analysis of the spontaneous clustering phenomena. Several techniques are to be employed to characterize the aspects of local and the macroscopic dynamics related to the synchronization clusters, capturing the mechanisms that allow them to arise and be maintained.

We consider a collection of N identical Fitzhugh-Nagumo excitable neurons perturbed by the white noise and interacting via the delayed linear couplings. Each neuron is connected to every other neuron, assuming uniform synaptic strength and the time-lag. Though the default setup involves a homogeneous ensemble, some of the cluster states are further shown to be robust with respect to small dispersions of the neuronal and network parameters. Results of the detailed numerical study on the properties of the cluster partition are discussed, making its dependence on the coupling strength, noise intensity, and the time-lag explicit. Following on that, we provide an explanation of the observed phenomena using numerical and qualitative arguments, as well as the recently developed mean-field model of the stochastic delay-coupled network of excitable units.^{22,28,34}

The paper is organized as follows. In Sec. II, the focus lies with the details of the applied neuron and population models, further providing background on the global regimes generic for the extended excitable media. Section III is aimed at introducing the coherence measure appropriate to characterize the mutual adjustment between the neuron firing patterns, arriving at the means to analyze the structure of clustered states from the macroscopic perspective. The other major issue concerns the relationship between the cluster states and the already familiar global regimes, in particular in terms of anticipating the parameter regions that may facilitate clustering. Section IV is dedicated entirely to the two-cluster states, examining whether and how are the regularity of local dynamics and the properties of cluster partition affected by variation of noise amplitude and the time delay. Another matter of interest is the asymptotic dynamics related to clustering, referring both to the long term stability and the behavior under increasing the system size. In Sec. V, one shows the structure of the three-cluster states to be prone to reconfiguration, at variance with its two-cluster counterpart. The two following sections underlie the common framework behind the clustering phenomena. On one hand, it is shown

that the coaction of noise and delay induces a unique form of neuron phase portraits, whereas on the other, the developed mean-field (MF) model is demonstrated to undergo a global bifurcation reflecting the onset of clustered states. The final section contains the summary and the discussion on the results obtained.

II. BACKGROUND ON THE NEURON MODEL AND THE POPULATION DYNAMICS

Consistent with the assumption on neuron excitability, the local dynamics of an N -size population is built on the Fitzhugh-Nagumo model^{35–37}

$$\begin{aligned} \epsilon dx_i &= (x_i - x_i^3/3 - y_i + I)dt + \frac{c}{n_i} \sum_{j=1}^N g_{ij} [x_j(t - \tau) - x_i(t)]dt, \\ dy_i &= (x_i + b)dt + \sqrt{2D}dW_i, \end{aligned} \quad (1)$$

where x_i and y_i are the respective activator and recovery variables, g_{ij} present the elements of the adjacency matrix and n_i refer to the number of neurons which the given neuron i is connected to. Setting $\epsilon = 0.01$ enforces a clear separation between the fast and slow variable subsystems, such that the former embodies the dynamics of membrane potentials, and the evolution of the latter may be linked to the action of the K^+ ion gating channels. The system is not subjected to external stimulation currents, so $I = 0$ holds. The neurons are nonetheless exposed to a noisy environment, a point reflected by the $\sqrt{2D}dW_i$ terms representing the stochastic increments of the independent Wiener processes, whose expectation values and correlations satisfy $\langle dW_i \rangle = 0$ and $\langle dW_i dW_j \rangle = \delta_{i,j}dt$. Communication between neurons occurs via diffusive couplings, parametrized by the synaptic strength c and the time delay τ , the latter accounting for the finite propagation speed over the axons and/or the latency in postsynaptic responses. The synaptic parameters are taken to be uniform not least for simplicity, but rather to set aside all possible sources of secondary effects that may interfere with the core clustering phenomenon.

The key intrinsic parameter b is supposed to modulate the neuron excitability. To see how this may be so, one first recalls how the isolated neuron in the noiseless case undergoes a supercritical Hopf bifurcation for $|b| = 1$, such that it possesses a unique attractor, the fixed point (FP) above and the limit cycle (LC) below this value. Appreciating the invariance of the system (1) to transformation $(x_i, y_i, b) \rightarrow (-x_i, -y_i, -b)$, one can consider only the case $b > 0$ without any loss of generality. As a corollary of the strong time-scale separation, the Hopf threshold marks the onset of relaxation oscillations, where the phase point within each cycle spends $O(1)$ time along the spiking and refractory branches of the slow manifold, executing rapid $O(\epsilon)$ jumps in between them, see Fig. 1(a). Translated to the stochastic version of the bifurcation, for vanishingly small D the trajectories still land on the appropriate attractor with probability 1.³⁸ However, slightly above $b = 1$ the neurons are found in an excitable regime, meaning that an adequate stimulation, be it by the noise or the interaction term, may elicit large transients of

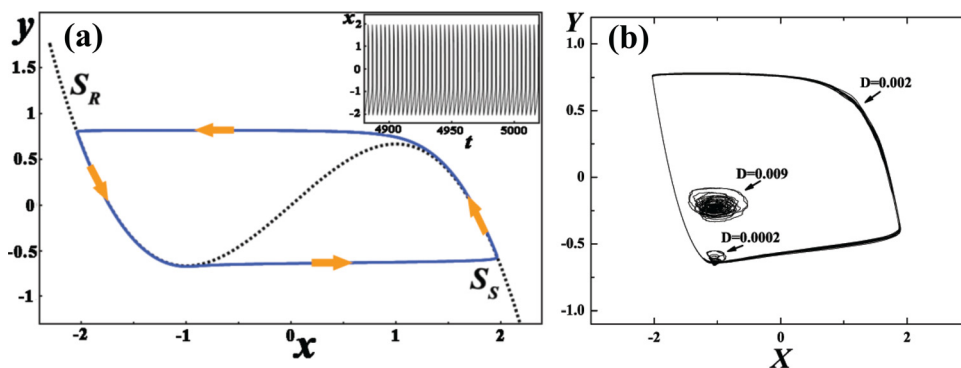


FIG. 1. Recap on the dynamics of an excitable Fitzhugh-Nagumo element, followed by an overview on the collective modes of excitable media, illustrated for the system 1 at $\tau = 0$. (a) In case of CR, the stochastic LC is a precursor to the deterministic one. As such, it takes place on the attractive (outer) branches of the x nullcline (dotted line), avoiding the unstable (middle) branch. EQ indicates the position of the equilibrium. A typical orbit (solid line) is made up of two portions of slow motion $O(1)$, connected by two rapid transients $O(\epsilon)$. The former include a descent down the refractory branch S_R until the left knee is reached, and the ascent along the spiking branch S_S . The inset shows a section from the time series $x(t)$ for $D = 0.003$. (b) For instantaneous couplings, the neural population exhibits three generic types of global behavior if D is systematically increased. This is epitomized by the phase portraits of the ensemble averages $X = N^{-1} \sum_{i=1}^N x_i$ and $Y = N^{-1} \sum_{i=1}^N y_i$ at $c = 0.1$, displaying incoherent motion ($D = 0.0002$), coherent collective oscillations ($D = 0.002$) and the decay into the chaotic regime ($D = 0.009$).

membrane potential, whereby the orbit traverses the spiking and refractory states before the equilibrium is reinstated. A typical instance of such a behavior is obtained for $b = 1.05$, the value kept fixed throughout the paper. Confined to the non-interacting case, one further encounters a range of intermediate noise amplitudes where the ensuing spike sequences show very little randomness. The particular setup with additive noise in the slow subsystem, such that in Eq. (1), may foster the coherence resonance (CR),¹⁹ characterized by a tight analogy between the stochastic LC and its deterministic counterpart.³⁹ The latter does not hold for the alternative scenarios attending noise in the fast subsystem: letting it act alone or combined with that in the slow variable dynamics may give rise to self-induced stochastic resonance (SISR)^{39,40} or several forms of mixed-mode oscillations,³⁸ respectively.

Extending the above framework to excitable media, one typically invokes a scenario where noise enacts a control parameter, tuning between the different global regimes.^{41–44} In case of instantaneous couplings, the ensemble averages have been demonstrated to take up three generic forms of behavior, contingent solely on variation of the noise amplitudes, as illustrated in Fig. 1(b). For small D , there is a stochastically stable global equilibrium, since the individual spiking is rare and incoherent, leaving most of the population at rest at any given time. The intermediate noise amplitudes give rise to a more frequent firing with most of the events synchronized, effectively turning the population into a macroscopic oscillator whose global frequency matches those of individual neurons due to mutual entrainment. Increasing D even further, one reaches a point when noise overwhelms the libration effects of coupling, with the ensemble averages decaying into chaotic regime. While the local spiking frequencies continue to increase, the synchronization systematically deteriorates by most of the spikes thrown out of step. These two points imply that at any instant the bulk of the population is refractory, which renders the trajectory of the global variables confined to an area of phase space much smaller than the one encircled by the LC.

The paradigm involving the three described types of behavior has first been reported for fully connected networks^{16,45} and has later been confirmed to endure for the layouts involving more complex interaction patterns.^{41,46} What we argue is that the inclusion of synaptic delay profoundly alters such a landscape, influencing in a meaningful way the succession of global variables' regimes. In particular, the coaction of noise and delay is found to facilitate a distinct form of synchronization that allows for the onset of the cluster states. As the effects of topology remain secondary to the core ingredients behind the phenomenon, namely, the noise, time delay and the neuron excitability feature, the results presented here refer to a globally connected network, viz., $g_{ij} = 1$ holds for each (i, j) pair of indices and $n_i = N$ applies to every node. This type of idealization has proven useful,^{47,48} and populations with assumed all-to-all couplings, once subjected to external forcing or feedback control, have even been implemented in modeling the emergence of healthy and pathological brain rhythms, as well as the interaction between the distributed brain areas.^{29,49,50} Nevertheless, in a discussion later on we consider an issue of removing a fraction of links between the neurons, showing that the phenomena laid out persist in randomly diluted networks on a condition that the sparseness level and the inhomogeneity in nodal degrees distribution are not excessive.

III. OBSERVATION OF CLUSTERING

The main topic of this section concerns introducing the appropriate tools to monitor the emergence and describe the temporal structure of the cluster states. In particular, there are four issues we address: first, defining the quantities that may readily be implemented to distinguish between the homogeneous and the cluster states; second, gaining an insight on the set of parameters that admit clustering; third, examining whether the cluster states appear monostable or coexist with the homogeneous ones, and fourth, devising methods to discern and visualize how the neurons get distributed between clusters for each realization of the n -cluster state. In

a nutshell, the aims stated are best achieved by means of pairwise and population coherence, which characterize the extent of correlation between the spiking events on the local and the global level.

To begin with, one is required to split the full iteration period T into bins k of length $\Delta = T/m$, such that each neuron i is awarded a binary variable $X_i(k) \in \{1, 0\}$, dependent on whether the neuron has fired or not within the given bin, respectively. By doing so, the continuous time series of neuron membrane potentials are coarse-grained into binary sequences of ones and zeroes. Then, the pairwise coherence κ_{ij} is defined as the cross-correlation between the neuron spike trains^{51,52}

$$\kappa_{ij} = \frac{\sum_{k=1}^m X_i(k)X_j(k)}{\sqrt{\sum_{k=1}^m X_i(k)X_j(k)}}. \quad (2)$$

Throughout the paper, the time bin $\Delta = 0.008$ is set, whereas $X_0 = 1$ is the threshold assigned for the neuron potential to cross so to register a spike, verifying that the results withstand if either of these values is reduced further. We have made certain that the transients are excluded from calculations. Note that the distribution of κ_{ij} values may be used to distinguish between the homogeneous and the (different types) of cluster states, the information gained from its modality and the peaks' width.

Alternatively, $\{\kappa_{ij}\}$ can also be viewed as if it provides a template for defining *a posteriori* a connectivity matrix completely independent on the structural one, given by g_{ij} . One may envision this as an interpolation of the notion of functional networks,^{53–56} a well-known tool for analyzing the properties of the long-term dynamics within the large N systems, essentially intended to qualify some form of synchronization between the units. This is based on the idea of

considering a pair of units (more strongly) coupled if their respective firing series are (better) synchronized. Hence, the way in which the functional network is built reflects the self-organization of neuron dynamics so that it places the units with precisely timed spikes within the same functional modules.^{29,53,55} The latter role is here assumed by the clusters, so that the functional networks can be applied in exposing the structure of the cluster states. Since we introduce the coherence as a type of synchronization measure, the terms functional and coherence network are used alternatively.

The coherence networks⁵⁷ referred to here are by construction undirected, but can involve either binary or weighted links. In the former case, a pair of neurons is considered connected if their pairwise coherence lies above a certain threshold Θ , be it nonzero or trivial.⁵⁶ Within this approach, the distinction between the homogeneous and the clustered states is apparent from the profile of the distribution of nodal connectedness degrees $P(k_i)$, as derived from the appropriate coherence network. Note that the nodal connectedness degree k_i is defined as the number of nodes which the given node i is connected to.

In Fig. 2(a), one sees the homogeneous state of global coherent oscillations typified by a unimodal distribution at $\Theta = 0$, such that all the neurons are interconnected, viz., the structural and the coherence networks are an exact match. On the other hand, for the cluster states, one expects an n -modal degree distribution $P(k)$, whereby the threshold level necessary to arrive at clearly separated peaks depends on the ratio of intra- to inter-cluster correlations: the higher it becomes, the lesser Θ is required. For the two-cluster state in Fig. 2(b), coherence between neurons participating the different clusters is negligible, so one may take a marginal threshold value to obtain the coherence network, whose nodal degree distribution reflects the cluster partition $\{N_1, N_2\}$.

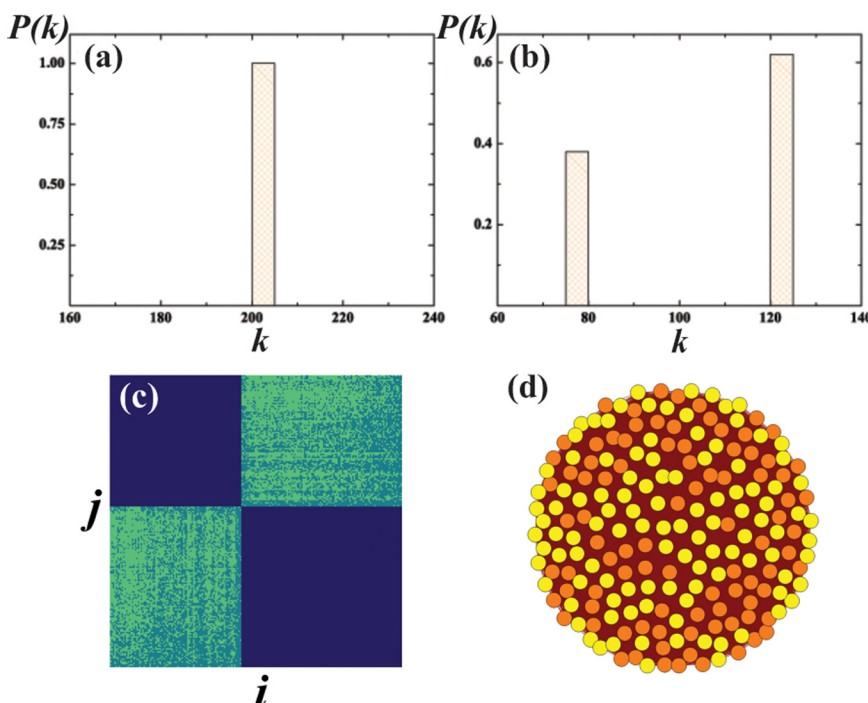


FIG. 2. Characterization of the cluster states in terms of features of the corresponding binary and weighted coherence networks. In (a) and (b), it is demonstrated how the distinction between the homogeneous coherent states and the n -cluster states can be made explicit by the binary coherence network, which possesses a unimodal (an n -modal) distribution of the nodal connectedness degrees $P(k)$ in the former (latter) case. The data in (a) are obtained for the homogeneous coherent state at $c = 0.1$, $D = 0.001$, $\tau = 6$, whereas the parameter values for the two-cluster state in (b) are $c = 0.1$, $D = 0.00025$, $\tau = 2$. The weighted coherence network, represented by the weight matrix in (c), and the binary network in (d) may serve independently or combined to capture the structure of the given cluster state, as shown for the two-fraction partition at $c = 0.1$, $D = 0.0005$, $\tau = 5$.

Now, let us explore the notion of the weighted coherence network, which rests on interpreting κ_{ij} as elements of a weight matrix that determines the scheme by which the nodes are interconnected. In order to visualize the structure of a cluster state, one is supposed to take two steps. The first is to introduce a distance metric which, loosely speaking, translates the least coherent neurons into the farthest ones, so that $\{\kappa_{ij}\}$ is effectively transformed into a matrix of distances $\{\gamma_{ij}\}$. The second step consists in applying an agglomerative hierarchical clustering algorithm on $\{\gamma_{ij}\}$, whereby the closest lying neuron groups are systematically merged into larger ones. Level-by-level, the groups to be joined are determined by a linkage criterion, expressing the intergroup distance as a function of pairwise distances between their respective members. In relation to the first step, it is convenient to adopt the distance metric $d(i,j) = 1 - \kappa_{ij}$. Completing the second stage, one readily obtains a dendrogram, where the layout of neurons in the lowest level may serve to rearrange $\{\kappa_{ij}\}$ so it assumes the block-diagonal form. The diagonal blocks mirror the clusters, and those off-diagonal represent the cross-correlations. What is displayed in Fig. 2(c) constitutes the outcome of the above strategy implemented in case of the two-cluster state obtained at $(D, \tau) = (0.0005, 5)$. A matter of some interest is to probe whether the binary and weighted coherence networks give rise to equivalent partitions for the same network state. Apparently, the binary networks, like the one in Fig. 2(d), provide less sophisticated information, but corroborate well with the weighted ones if the clusters are well separated, viz., when Θ should top only the very small cross-terms. Once there is more ambiguity to the separation, reaching the qualitative agreement rests with selecting the “proper” Θ for the binary network, as we see later on.

A. Where to look for the cluster states?

Having discussed the means of characterization, the next objective is to determine the parameter domains that facilitate the onset of the cluster states. For the most part,

one is interested in the impact of D and τ , and to a lesser degree in the influence of c . Focussing initially on the isolated effects that each of the parameters brings in, we first consider how the system’s behavior is modified under variation of a single parameter, while the remaining ones are fixed. To this end, one invokes the global coherence⁵² $\kappa = \frac{1}{N(N-1)} \sum_{i,j=1;i \neq j}^N \kappa_{ij}$, derived from the pairwise coherence by averaging over the neuron population. Given the definition, κ may assume values within the $[0, 1]$ interval, with the upper and lower limits reflecting the completely coherent and incoherent firing between neurons, respectively. What is most useful about κ is that it decreases only for two reasons, either if the cluster states emerge or if some form of disordered states sets in. In the former case, should there be a two-cluster state with an approximate equipartition and a strong cluster separation, one expects to find $\kappa \approx 0.5$ or a slightly lesser value, depending on the deviations from the two assumptions we made. However, a larger reduction of κ can be considered a certain signature of the disordered states. Based on these two remarks, one should be able to read from any κ dependence where the cluster states are likely located. In particular, if there are no disordered states in the vicinity, the cluster states should coincide with the local minima of κ .

This is first probed for the $\kappa(\tau)$ dependence, viz., Fig. 3(a), having D fixed at two appropriate values, $D_1 = 0.0005$ and $D_2 = 0.0007$. Under this setup, the intention is to demonstrate that tuning the delay gives rise to the clustering effect, meaning that there exist some narrow intervals of τ which may be cast as the *cluster-resonant* ones.³³ We have indeed found by numerical simulation that the local minima around $\tau \approx 2, 6$ and 10 coincide with the onset of the two-cluster states, as to be expected from the curves’ profile. The properties of such states will be analyzed in more detail in Sec. IV. However, one notes that clustering around $\tau \approx 2$ is distinct from the analogous phenomena for larger τ , given that in the former case, when increasing the delay, no homogenous coherent states arise prior to the cluster state, a point which in the latter case no longer applies. The other

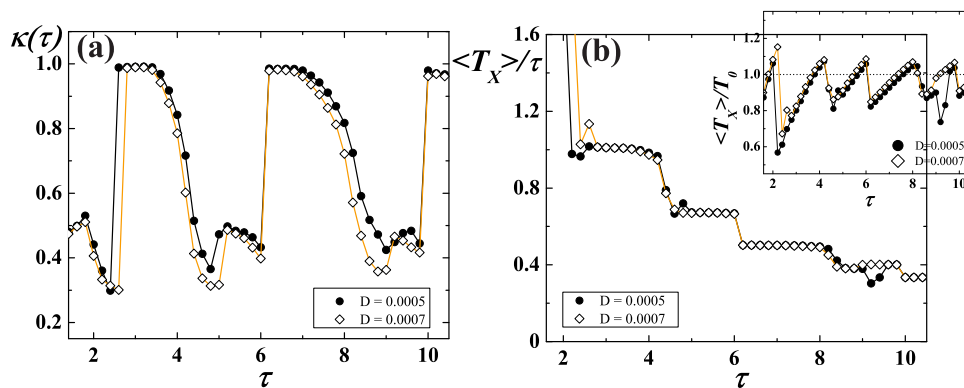


FIG. 3. Focus on the impact of interaction delay on the system’s behavior. (a) shows the $\kappa(\tau)$ plots for $D = 0.0005$ (solid circles) and $D = 0.0007$ (open diamonds) at fixed $c = 0.1$. The local minima exhibited by $\kappa(\tau)$ serve as an indication on the intervals of τ that foster the cluster states. (b) The representation scheme with respect to D is adopted from (a). The inset refers to the variation of the average oscillation period $\langle T_X \rangle / T_0$ with τ for the macroscopic variable X . In qualitative terms, the curves appear virtually the same for different noise, whereby the given profiles imply that the system’s dynamics can be traced to the competition between the noise-driven and the delay-driven oscillation modes. The dashed line corresponds to the case $\langle T_X \rangle = T_0$. In the main frame is displayed the dependence of the scaled average oscillation period $\langle T_X \rangle / T_0$ on τ for different D . For the homogeneous coherent states found within the approximate intervals $\tau \in [2.6, 4.2]$, $\tau \in [6.2, 8.2]$ and $\tau \geq 9.8$, the above competition is resolved in favor of the delay-driven mode. For the two-cluster states around $\tau \in [4.8, 6]$ and $\tau \in [8.8, 9.8]$, the noise-driven mode prevails.

important observation is that $\kappa(\tau)$ acquires virtually a universal form for the fixed D values selected from the range relevant to clustering. The minor differences around the local minima are the reflection of the noise-specified behavior of the global variables leading in to the formation or dissipation of the cluster states. Such background effects lie outside the scope of the present paper. However, the argument on minor differences and the earlier statements on having to select the appropriate D values that admit clustering imply that one should also take into account the interplay between the effects of D and τ . In particular, apart from the characteristic time-scale determined by τ , note that the noise intensity as well brings in a characteristic time-scale, the one for “bare” oscillations in the delay-free case $\tau = 0$. The latter’s period T_0 is solely determined by D , with $T_0(D)$ being a decaying function within the considered D -range. To get a sense on the values which T_0 may assume, we state two relevant instances, $T_0(D = 00005) \approx 3.78$ and $T_0(D = 00007) \approx 3.66$. It is not a surprising effect to find the system’s behavior being determined by the competition between the two oscillation modes, one guided by noise and the other driven by the interaction delay. In this context, it is interesting that the cluster-resonant delays τ_r in Fig. 3(a) may roughly be approximated by the formula $\tau_r = T_0/2 + n * T_0$, which contains an implicit dependence on D through τ . Note that the given expression is similar to what is obtained in Ref. 58 for the coupled phase oscillators. Nevertheless, the formula may only be accepted in conditional terms, under two important constraints. First, it should not be read as if implying the existence of point-like resonances with delay, but rather as an indication on where the centers of the cluster-resonant intervals are situated. On the second constraint, note that Fig. 3(a) has the formula empirically confirmed only for $n = 0, 1, 2$. However, one should also take into account that considering overlong delays, viz., τ several times longer than the neuron refractory period, makes little sense in physiological terms.

Looking for further confirmation and additional details on how the system’s behavior is driven by the competition of the delay and noise-driven oscillation modes, we examine the variation with τ of the normalized average oscillation period for the global variable X , $\langle T_X \rangle / T_0$, where averaging refers to an ensemble of different stochastic realizations. The plot is displayed in the inset of Fig. 3(b). Determining $\langle T_X \rangle$ is the same as determining the average interspike interval (ISI),⁵⁹ except for the two-cluster states, where the former is approximately twice as the latter. Apart for the non-trivial behavior in general, the curves for different D again qualitatively show a common form, with the minor noise-specific effects manifested mostly in the vicinity of $\tau \approx 2$. An important point is that around τ_r the $\langle T_X \rangle / T_0$ values lie very close or slightly above the identity line $\langle T_X \rangle = T_0$, indicated by dashes in the inset of Fig. 3(b). This should not be confound with the peaks around $\tau \approx 3.8$ and $\tau \approx 7.6$, where $\tau \approx n * T_0$ applies. These peaks are unrelated to clustering and reflect a form of global events in the phase space, which involve the limit cycle for the macroscopic variables approaching the vicinity of the saddle fixed point. Nonetheless, once the homogeneous coherent states first set in ($\tau \gtrsim 24$), $\langle T_X \rangle / T_0(\tau)$ dependence exhibits nearly a periodic behavior

approximately respecting the bare oscillation period T_0 , viz., the sections $\tau \in [2.6, 6.2]$ and $\tau \in [6.2, 9.8]$.

To establish more firmly how are the homogeneous and the cluster states distinguished in terms of the prevailing oscillation modes, we also consider the variation with τ of the scaled average oscillation period for the global potential, $\langle T_X \rangle / \tau$, see the main frame in Fig. 3(b). It strikes that the curves for different D again show nearly universal behavior. Essentially, one finds three plateaus approximately for $\tau \in [2.6, 4.2]$, $\tau \in [6.2, 8.2]$ and $\tau \gtrsim 9.8$, which are numerically confirmed to coincide with the homogeneous coherent states. Their average oscillation periods amount to τ , $\tau/2$ and $\tau/3$, respectively, clearly implying the prevalence of the delay-dominated mode over the noise-driven one. Cross-referencing the results from the inset and the main frame, it also becomes clear that the sections for the approximate intervals $\tau \in [4.8, 6]$ and $\tau \in [8.8, 9.8]$ correspond to the two-cluster states, where the T_0 -dominated oscillation mode wins over the τ -dominated one. In other words, it may be stated that in the noise-delay adjustment leading up to the cluster states, noise has the upper hand on determining the oscillation frequency, suppressing the forcing effect of the delay. As for the impact of bringing in the stronger noise, one only observes a minor broadening of the τ intervals where clustering can be found. This may be interpreted in the context of the finding that the delay-driven mode gives way to that driven by noise when the cluster states set in. Though it presents a simplification, note that the approximate formula on $\tau_r(T_0)$ is able to capture how the centers of the cluster-supporting delay intervals shift to smaller τ for larger D .

After an extensive overview focused mainly on the effects of τ on the formation of the cluster states, we direct our attention to demonstrating more explicitly how the system’s behavior is influenced by the variation of D . In this context, it is interesting to compare the $\kappa(D)$ curves for the different τ , examining how the cluster states interfere with the previously known picture involving three generic global regimes, contingent on the intensity of noise. To this end, in Fig. 4(a) are displayed the $\kappa(D)$ curves obtained by having fixed the delays at $\tau = 2, 4$ and 6 . The value $\tau = 2$ has earlier been established to support clustering, $\tau = 6$ is in this respect marginal but still facilitates the cluster states, whereas $\tau = 4$ is identified as the value where no cluster states emerge. The latter curve serves to provide the point of reference, given that the deviations from its form may indicate clustering, among other phenomena. Note that the curve $\tau = 4$ conforms to a stereotype profile in the delay-free case $\tau = 0$. Following the explanation on the global regimes stated in the Introduction, one would expect to be able to discern three segments for the small, intermediate and large values of D , coinciding with the low initial κ values, significant κ increase through the middle section and a sharp decay for the latter part. This is basically confirmed for $\kappa(D)$ at $\tau = 4$, only the initial segment with low values is not apparent, as the required noise amplitudes are much smaller than the adopted, already small sampling step for noise. Note that the $\kappa(D)$ curves for $\tau = 2$ and $\tau = 6$ acquire quite different forms, though they both indicate clustering at certain D ranges. In the former case, $\kappa \approx 0.5$ implies the existence of two-cluster states for

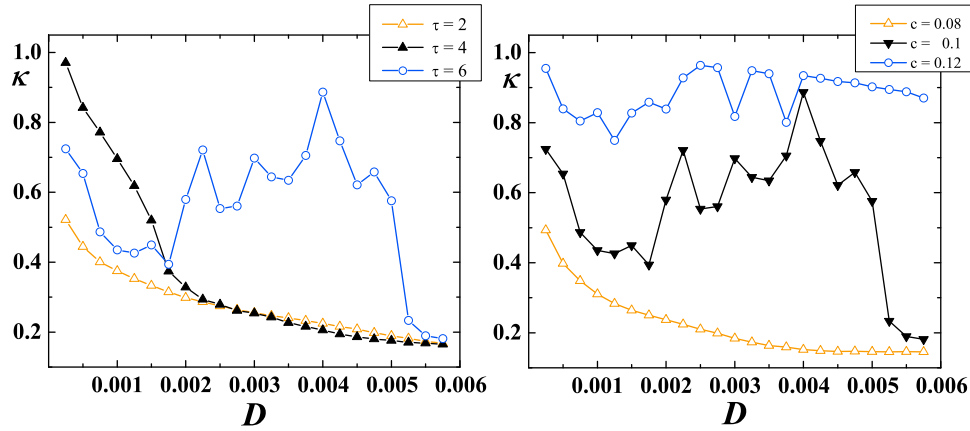


FIG. 4. Insight on the impact of D and c on the system's dynamics. (a) shows the $\kappa(D)$ family of curves for the set of delay values including $\tau = 2$ (open triangles), $\tau = 4$ (solid triangles), as well as $\tau = 6$ (open circles), having $c = 0.1$ fixed. Two-cluster states are indicated for the noise amplitudes $D \lesssim 0.0008$ at $\tau = 2$, whereas the appropriate range of D is broader at $\tau = 6$. The curve's profile for $\tau = 4$ implies the lack of clustering within the considered interval of noise. (b) illustrates how the shape of the $\kappa(D)$ curves at fixed $\tau = 6$ is altered under variation of c , beginning with $c = 0.08$ (open triangles), over $c = 0.1$ (solid triangles) to $c = 0.12$ (open circles). Too strong a coupling appears to suppress the onset of the cluster states.

relatively small $D \lesssim 0.0008$. In the case $\tau = 6$, the D values that foster clustering seem to span the wider range. However, the overall picture may be somewhat smeared, since some average κ do not correspond to either the homogeneous coherent or the cluster states, reflecting bistability between the two, or even other types of multistability within some parameter ranges.

Finally, we touch upon the influence of varying the coupling strength c on the formation of the cluster states. To do so, we plot the $\kappa(D)$ families of curves for $c = 0.08$, 0.1 , and 0.12 at fixed $\tau = 6$, see Fig. 4(b). It is apparent that the stronger the coupling, the more isolated become the “irregularity” sections embedded into the flatter curve's profile, the latter being a corollary of the interaction term winning over the noise. Put differently, the stronger coupling confines the cluster states to smaller regions of the D - τ parameter space, making the resonance effect a more sharper one.

Once the existence of cluster states is established, κ may be put to use in determining whether they appear monostable or the dynamics exhibits multistable behavior for the given parameter set. If the κ values for different stochastic realizations were to bunch into distinct groups, it should be considered an evidence of the latter. On a cautionary note, this issue is likely to be sensitive on the system size.

Unless stated otherwise, the results presented throughout the paper refer to a population of $N = 200$ neurons, with the numerical integration performed by an Euler method taking the iteration step $\delta t = 0.002$. Additional reduction of δt has been confirmed to leave the results unaffected. Apart from direct simulations of the ensemble dynamics for $N = 500$ and $N = 700$, the persistence of clustering phenomena has been verified by a method intended to probe the asymptotical behavior of the system in the thermodynamic limit $N \rightarrow \infty$, see Subsection IV A. The two sections to follow are aimed at characterizing the temporal structure of the two- and three-cluster states. The former are demonstrated to be stationary and the latter dynamical by nature,⁶⁰ the distinction based on whether the neurons are allowed to cross back and forth between the clusters.

IV. PROPERTIES OF THE TWO-CLUSTER STATE DYNAMICS

Enhancing the noise amplitude, the two-cluster states are first encountered at $D \approx 0.00025$ for $\tau = 2$. It is noteworthy that the given D values lie close to the crossover domain between the incoherent and the coherent collective dynamics. A useful approach is to consider first the phase portrait for the macroscopic variables $X = N^{-1} \sum_{i=1}^N x_i$ and $Y = N^{-1} \sum_{i=1}^N y_i$, deemed as suitable descriptors since the higher amplitude of the peak global potential reflects a larger portion of neurons firing in synchrony. For such collective motion, Fig. 5(a) yields a twisted orbit made up of two clearly discernible segments that coincide with the macroscopic fractions of the population activated in turns, whereby the approximate synchronization within the subsets is maintained. In other words, the structureless population is in a dynamical fashion split into clusters, such that one's activation is accompanied by the neurons in the other cluster being refractory. This goes along with the observation in Fig. 5(b), demonstrating the overlap between the $X(t)$ spikes and the individual action potentials evoked in arbitrary neurons from the distinct clusters. One also learns how each of the two latter series displays high regularity, with the phase difference between their respective pulses apparently locked to π . The particular phase shift implies a splay state,^{12,61} meant in general as an n -cluster partition where the phase difference between any two groups amounts to an integer multiple of $2\pi/n$.

To display the above behavior, the neurons have to be entrained to a single frequency, a point reflected in the distribution of local jitters r_i ^{19,46} over the population. The jitters are defined as normalized variations of the interspike intervals T_k extracted from the individual time series x_i

$$r_i = \frac{\sqrt{\langle T_k^2 \rangle - \langle T_k \rangle^2}}{\langle T_k \rangle}, \quad (3)$$

such that their smaller values indicate more regular firing patterns. Expectedly, for $(D, \tau) = (0.00025, 2)$, the r_i distribution in Fig. 6(a) is unimodal with a narrow peak and a

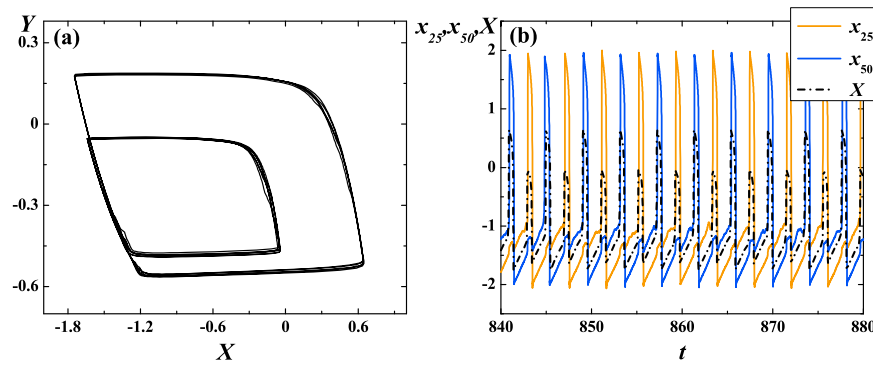


FIG. 5. Two-cluster states at small D and τ . (a) As a signature of the population split, the phase portrait for the collective dynamics shows a twisted limit cycle orbit, where the two discernible segments reflect the action of the clusters. (b) A section from the $X(t)$ series (dashed line) is overlaid by the $x_i(t)$ series (solid lines) for two arbitrary neurons from the distinct clusters. A high-level coherence within the subsets is witnessed by the fact that the peaks of the global potential perfectly match the ones of the local potentials. The latter series imply that the firing of clusters is locked in antiphase. The data are provided for the case $c = 0.1$, $D = 0.00025$, $\tau = 2$.

maximum at a very low value $\langle r_m \rangle \approx 0.01$, all the points indicative of the approximately uniform neuron frequencies across the population. Also, the mutual interaction acts within the clusters so to give rise to a form of a recovery mechanism, which rapidly suppresses any neuron from displaying large fluctuations in the firing period, the type of behavior that potentially leads to escaping the cluster. Though the stochastic background of the system dynamics may resurface causing occasionally the local ISIs to depart noticeably from the mean, one finds such perturbations resolved already in the next firing cycle. This is witnessed in Fig. 6(b), where the first return map of the ISIs for an arbitrary neuron shows a large majority of points tightly bunched. The latter holds irrespective of the cluster the given neuron belongs to, the point confirmed by the virtually indistinguishable ISI distributions for the members of the distinct subsets, *viz.*, the inset in Fig. 6(b).

In terms of variations of the two-cluster partition $\{N_1, N_2\}$ under different stochastic realizations, it is interesting how for small D and τ the system appears less disposed to a splay state with equal sized fractions. Instead, one finds the fractions' ratio fluctuating around 2:1, displaying the stronger convergence to an asymmetrical state if the population size N were increased, which rules out the possibility of

this being the finite-size effect. In fact, it has more to do with the reduced ability of small amplitude noise to draw more neurons away from the main bunch.

At certain τ longer than the average cycle of the isolated neuron, the two-cluster states are found to span the range $D \in (00004, 00008)$, a domain where the homogeneous coherent states are obtained in the case $\tau = 0$. Though at first sight of Fig. 7, illustrating the typical phase portrait for the ensemble averages under these parameters, it may seem plausible just to carry over the arguments from above, one should still outline a couple of differences. On a lesser note, the maximum of the r_i distribution is seen to shift to $\langle r_m \rangle \approx 0.19$ due to an overall reduced regularity of the firing patterns. Qualitatively, however, the system dynamics in respect to different stochastic realizations switches into a bistable regime which involves coexistence between the two-cluster and the disordered states. Also, the conditions where D and τ are increased seem to favor the symmetrical cluster state with equal fractions in the population partition. The tendency to $N_1/N_2 \approx 1 : 1$ ratio becomes more salient with the increased system size, but is manifested as well for a somewhat larger $\tau = 6$, if the D values lie in the already considered range.

Though it is not within the scope of the present paper to extend the analysis in such a direction, one should still verify

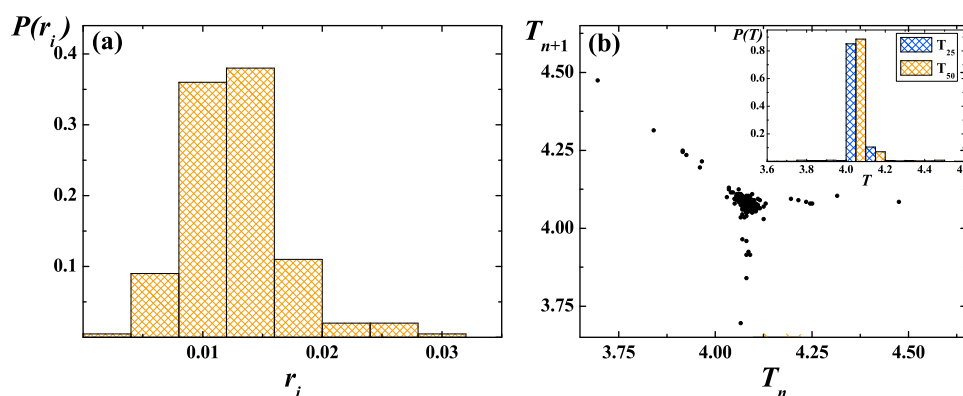


FIG. 6. Properties of single neuron dynamics. (a) The distribution of local jitters $P(r_i)$ implies that highly regular spiking patterns are maintained across the ensemble. (b) The first return map of the firing periods T_n for an arbitrary neuron illustrates how any larger deviations from the mean value are rare, further subdued already within the following cycle. The latter is upheld independent on the particular cluster a neuron belongs to. This is witnessed in the inset, which shows the ISI distributions $P(T_n)$ for two arbitrary neurons from the distinct subsets. The parameter set is $(c, D, \tau) = (0.1, 0.00025, 2)$.

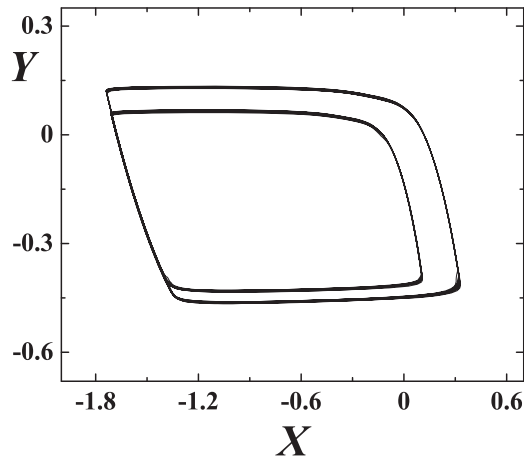


FIG. 7. Two-cluster states at intermediate D and τ . Phase portrait for the global dynamics at $(c, D, \tau) = (0.1, 0.0005, 5)$ is projected in the $X - Y$ plane. The properties of the cluster partition N_1, N_2 are seen to depend on the parameter values, whereby the larger D and τ appear to favor the states closer to an equipartition $N_1/N_2 \approx 1 : 1$ over the asymmetric clustering.

that the two-cluster states remain intact if one were to introduce heterogeneity into the intrinsic neuron parameters or the network coupling scheme. On the former, we have considered a population diversity scenario⁶² where the excitability parameter is randomly drawn from a uniform distribution over a 2σ interval around $b = 1.05$. One should be careful to adjust σ so that the lowest possible b lies above the Hopf threshold $b = 1$. Nevertheless, the ensuing phase portraits for $(c, D, \tau) = (0.1, 0.00025, 2)$ and $(c, D, \tau) = (0.1, 0.0005, 5)$ are virtually unchanged compared with those in the homogeneous case, except for the minor variations in the cluster sizes occurring sporadically between the firing cycles. The other point concerns the persistence of the two-cluster states in case when the embedding network is randomly diluted. The dilution is carried out by randomly removing a certain

fraction of links (synapses) from the fully (globally) connected network, as defined by the probability for removal p . Expectedly, at the above (c, D, τ) parameter sets we have found no modifications in the collective dynamics for the moderate p , say $p = 0.3$ or slightly above.

A. Asymptotic dynamics

This subsection covers the asymptotic dynamics related to the two-cluster state, both with respect to the long-term behavior and the increasing system size. On the former, one may inspect how are the representative points of neurons distributed in the $x_i - y_i$ phase space at different moments over the sufficiently long iteration period, viz., Fig. 8. This is helpful in demonstrating the persistence of clusters, especially their invariance to dissolution and reconfiguration. The two representative clouds can be seen to maintain a clear separation and compactness throughout the simulation, as they should if the neurons are indeed forbidden to leave and exchange clusters. In practice, to assert the latter one may further select a triplet of neurons, where a couple belongs to the same cluster, and then show how these two are always clumped together, while the remaining neuron never has the spikes synchronized with them. This is further elaborated in Sec. V A, where the method of dynamical correlation coefficients is implemented.

So far, the arguments on the persistence of cluster states with increasing N have relied on the results of numerical simulations. Here, we implement a method intended to probe the system dynamics in the thermodynamic limit $N \rightarrow \infty$. To this end, one introduces a type of a synchrony measure⁶³

$$\chi^2(N) = \frac{\sigma_X^2}{\frac{1}{N} \sum_{i=1}^N \sigma_{x_i}^2}, \quad (4)$$

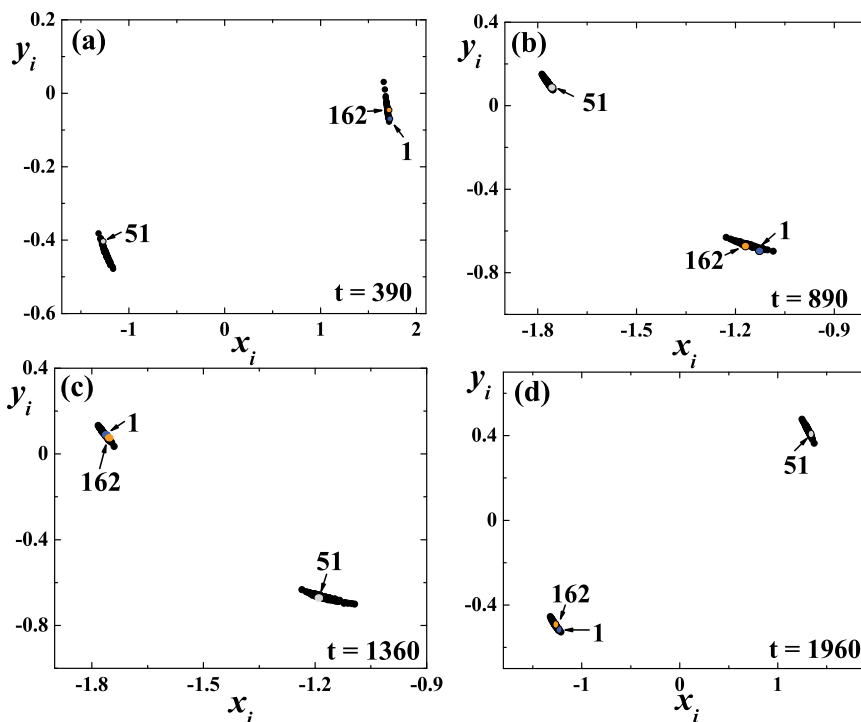


FIG. 8. In case of the two-cluster state, evolution of the representative clouds for the distinct clusters is shown in the $x_i - y_i$ phase space. To indicate the stationary character of the cluster partition, we selected a triplet of neurons, including two arbitrary members (labeled by 1 and 162) from one cluster, and a single neuron (labeled by 51) from the other cluster. At any given moment, the neurons' respective positions, denoted by arrows, imply that there is no mixing between the clusters. The parameters are set to $(c, D, \tau) = (0.1, 0.0003, 2)$.

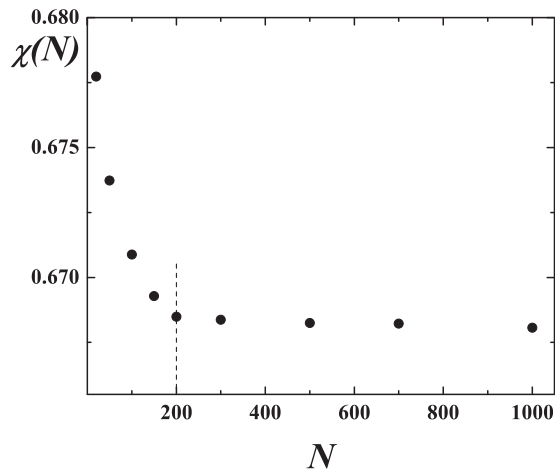


FIG. 9. $\chi(N)$ dependence for the two-cluster state at $(c, D, \tau) = (0.1, 0.0005, 5)$. The existence of an asymptotic component $\chi(\infty) \in (0, 1)$ suggests the persistence of clustering in the thermodynamic limit, whereby the onset of the near-asymptotic behavior is found about $N \approx 200$. The latter makes it unlikely that the stability of the two-cluster states in larger populations may be altered by some mechanisms absent at smaller N .

which presents the time-averaged variance of the global potential $X(t)$, $\sigma_X^2 = \langle X(t)^2 \rangle_t - \langle X(t) \rangle_t^2$, normalized over the mean of the time-averaged variances of the local potentials $x_i(t)$, $\sigma_{x_i}^2 = \langle x_i(t)^2 \rangle_t - \langle x_i(t) \rangle_t^2$. By the law of large numbers, for the systems of sufficient size $\chi(N)$ reads⁶³

$$\chi(N) = \chi(\infty) + \frac{a}{\sqrt{N}} + O(1/N), \quad (5)$$

where $\chi(\infty)$ denotes the asymptotic component. Should there be genuine cluster states, the latter is expected to lie within a range between 0 and 1. The existence of the $\chi(\infty)$ term has been verified for the previously considered parameter sets, with the example for $(D, \tau) = (0.00025, 2)$ provided in Fig. 9. Notably, the $\chi(N)$ dependence makes it explicit that the near-asymptotic behavior sets in already about $N \approx 200$. This suggests that the implied stability of the two-cluster states in large populations cannot be affected by some mechanisms absent at small N .

V. THREE-CLUSTER STATE DYNAMICS

The cluster states addressed so far can be considered stationary in terms of stability against reconfiguration, which is the changes in population partition due to neurons switching

back and forth between the clusters. Adding up to a polymorphous character of the clustering phenomena, we also report on the existence of three-cluster states dynamical by nature,⁶⁰ where the ability of neurons to exchange cluster survives even in the asymptotic regime. One stresses how such a scenario, encountered with further increase of D and τ about $D \approx 0.0013$ for $\tau = 10$, does not include a splay state with the clusters at any moment staggered by the $2\pi/3$ phase difference, so it should by no means be related with stochastic fluctuations around such a partition. Instead, there is a weaker cluster separation, which is best analyzed applying the methods laid out in Sec. III, drawing a comparison to the results on the properties of binary and weighted coherence networks derived in Sec. IV.

In particular, the pairwise coherence matrix in Fig. 10(a) yields the inter-cluster elements much larger than those in the two-cluster state. A further indication on this is received from the corresponding binary network, whose structure now shows a strong dependence on the threshold parameter Θ , a point announced earlier on. If one chooses too low a threshold, there is insufficient resolution to distinguish between the three clusters, so one may end up with a seemingly two-cluster partition. However, any choice of Θ should be justified in a self-consistent fashion, such that no qualitative changes emerge after it is increased. In this context, it may readily be verified how a rise in Θ reveals the actual three cluster partition, viz., Fig. 10(b), corroborating with the findings from the coherence matrix approach.

Now let us focus on the origin and the long term behavior of the three-cluster states. In relation to the former, an important perspective lies with the local dynamics. Except for the brief episodes within the population cycle when all the units are refractory, at any given moment the three clusters are roughly made up of neurons in refractory, spiking and resting (excitable) states, respectively, whereby the two latter subsets are proximal in the phase space. For this point alone, the three-cluster state may best be understood as derived from the two-cluster state instability, where the mutual entrainment fails to maintain the proper inter-cluster phase difference, giving way to noise. Moreover, the instability is self-sustained, as the stochastic effects are amplified by the very properties of the partition that has two subsets firing in close succession. Note how for any neuron participating in the cluster states there are but two effective sources of noise, one explicit, embodied by the D term in the y_i subsystems,

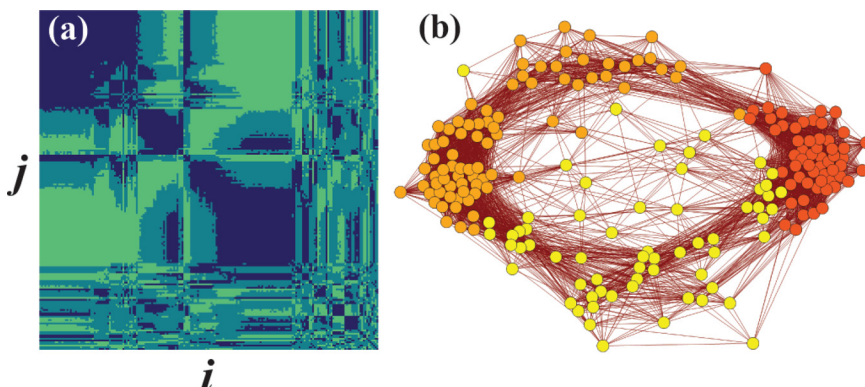


FIG. 10. Global properties of the three-cluster state. (a) Compared to Fig. 2(c), the weight matrix for the weighted coherence network displays larger off-diagonal terms, indicating less clear cluster separation. (b) The binary coherence network reveals the three-cluster partition if the threshold level is raised to $\Theta \geq 0.45$. The data refer to the parameter set $(c, D, \tau) = (0.1, 0.0013, 10)$.

and the other implicit, due to interaction in the fast variable subsystems. On the latter, consider first the example involving the two-cluster partition. There, one finds a kind of subdivision imposed between the interaction terms, such that each neuron feels the action of its cluster co-members strongly, while the impact of the other subset amounts to noise, which is a consequence of tuning between the delay and the duration of neuron firing cycles. To some extent, this carries over to the three-cluster state. In particular, the intra-cluster interactions still provide “periodical forcing” necessary to conserve the mutual entrainment, whereas the action of neurons from the other two clusters may be treated, apart for some zero-measure intervals due to imperfect adjustment of spiking periods relative to τ , as interaction-induced noise with zero mean values and small amplitudes. Nevertheless, the combined effects of the enhanced noise “proper” and the “interaction noise” can make an excitable neuron susceptible to exchanging clusters. This can take place under the scenarios of “spike skipping” or “premature firing.” In the former case, a neuron is denied a spike by getting caught in vicinity of the equilibrium, so that it misses out on its cluster beat. In the event of premature firing, a sufficiently large interaction term influences a neuron passed beyond the halfway of the mean interspike interval, making it escape the refractory branch of the slow manifold. Once the given unit discharges ahead of the remaining subset co-members, there is a high likelihood for it to become assimilated into the cluster active around that time.

An intuitive perspective on the long-term behavior behind the three-cluster states may be gained by considering the features of the appropriate r_i distribution (not shown). Two points deserve special attention, both at odds with what is obtained for $(D, \tau) = (0.0005, 5)$. First, the distribution peak is around $\langle r_m \rangle \approx 0.09$, the value substantially higher compared to 0.19 from the previous case, and second, the distribution has a longer tail to the right. The former is not easy to grasp, as it can hardly be attributed solely to a $D - \tau$ co-effect. In view of the very narrow D interval occupied by the three-cluster state, one may rather hypothesize a more subtle development, a putative interplay between the noise proper and the interaction-induced noise, which is not too far off the scenarios for the mixed-mode oscillations exhibited by isolated neurons subjected to additive noise in both the fast- and slow-variable subsystems. As for the longer tail of the r_i distribution, the three-cluster partition apparently exhibits a form of disorder related to the broken balance between the refractory and the spiking branches of the population at any given moment. This is likely to make the state non-generic, meant as sensitive to all kinds of parameter inhomogeneities, including the nonuniform connectivity patterns and the diversity introduced by letting b vary over the ensemble.

From the analysis of the available mechanisms by which the neurons exchange clusters, as well as the findings on the r_i distribution, it is justified to conclude that the gross-structure of the three-cluster states involves a nucleus made up of two clusters and a non-negligible fraction of “itinerant” neurons, switching between the hard cores. This is not to say how the former are free from cluster exchange, it is only that

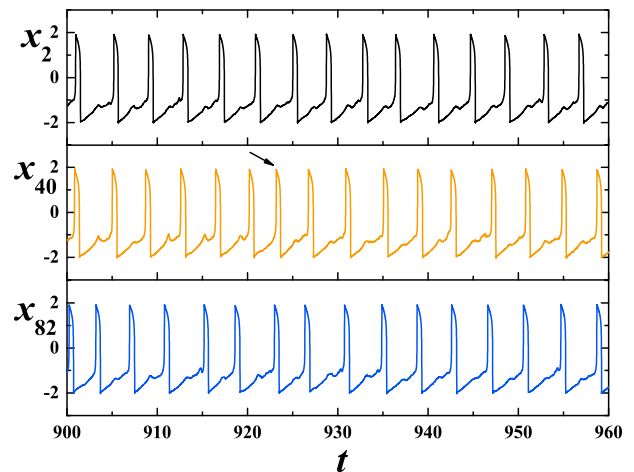


FIG. 11. Illustration of the dynamical clustering typifying the three-cluster states. The top and bottom panels show sections from the $x_i(t)$ series for two arbitrary neurons, labeled 2 and 82, which belong to distinct core-clusters. The middle panel refers to a minority subset that exhibits switching between the cores, with its behavior characterized by the neuron 40. Within the interval $t \in [900, 922]$, spiking in the middle series is in step with the top series, whereas for $t \in [923, 960]$ it is synchronized with the firing series from the bottom panel. The moment when the neuron 40 jumps between the two core-clusters $t \approx 922$ is indicated by an arrow in the middle panel. The data are provided for $(c, D, \tau) = (0.1, 0.0013, 10)$.

on the average they execute considerably less jumps than the latter. An instance showing one of the itinerant neurons switching between the core clusters via the “premature firing” scenario is provided in Fig. 11. Curiously enough, in spite of being involved in an apparently random activity, the itinerant neurons do not behave in an independent fashion but rather maintain some degree of mutual coherence. In terms of the corresponding distribution of local jitters, the nucleus comprises the values centered around its peak, whereas the rest of the population reflects its tail. Altogether, both the intra- and the inter-cluster synchronizations are intermittent by nature, but the neurons with more frequent coherent episodes are more likely to commit to synchronous firing again.

A. Dynamical correlation coefficients as means to quantify dynamical clustering

Appreciating the discussion above, we implement a method illustrative of the extent of co-activity which qualifies the neurons as members of the same cluster. Focusing on characterization of the coherent episodes, one considers the evolution of the dynamical correlation coefficients⁶⁴

$$c_k^{ij} = \frac{\langle T_i T_j \rangle_k - \langle T_i \rangle \langle T_j \rangle_k}{\sqrt{(\langle T_i^2 \rangle_k - \langle T_i \rangle^2)(\langle T_j^2 \rangle_k - \langle T_j \rangle^2)}}, \quad (6)$$

each reflecting the variation of the pairwise correlation between the respective ISIs sampled over the moving frame. The frame’s length should scale with the characteristic duration of the episodes or be taken so to encompass a meaningful number of events, say in the range of tens of spikes. In Eq. (6), T_i and T_j denote interspike intervals for neurons i and j , whereas the angled brackets indicate averaging over

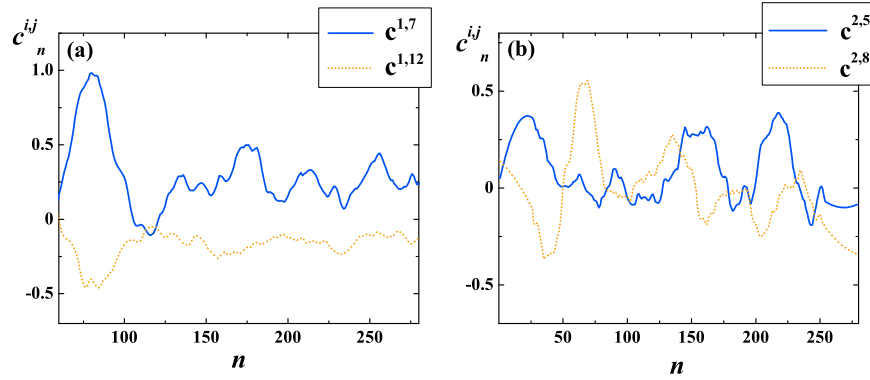


FIG. 12. Asymptotic vs intermittent synchronization between the neurons. (a) and (b) refer to the two-cluster state at $(c, D, \tau) = (0.1, 0.0005, 5)$ and the three-cluster state for $(c, D, \tau) = (0.1, 0.0013, 10)$, respectively. In both panels are plotted the time variations of c_k^{ij} for an arbitrary pair of neurons in the same cluster (solid lines) and from the distinct clusters (dotted lines). (a) implies stable correlated (anti-correlated) spiking within (between) the subsets. The mixed picture in (b) indicates that correlated episodes occur for neurons occupying both the same cluster and the distinct ones, but are more abundant in the former case. The smoothed curves are obtained by applying the second-order Savitzky-Golay algorithm.

the k -th frame. c_k^{ij} belong to the interval $(-1, 1)$ and highlight how well are the fluctuations in firing patterns of one neuron matched by those of the other on a low level of temporal coarse-graining. The values close to the upper (lower) boundary indicate correlated (anti-correlated) spiking, while near zero values point to the lack of correlation.

In Fig. 12, the objective is to clearly distinguish between the asymptotically stable two-fraction and unstable three-fraction partitions by plotting side-by-side the c_k^{ij} time dependencies which illustrate the typical inter-cluster (dotted lines) and intra-cluster (solid lines) correlations. The (i, j) couples for each partition are chosen so to keep one neuron fixed, while extracting from its own and the distinct cluster the other neuron. If large fluctuations in c_k^{ij} are encountered, one may resort to an appropriate smoothing algorithm. As expected, in Fig. 12(a) which refers to the two-cluster state, there is persistent correlated (anti-correlated) spiking within (between) the clusters, whereby the corresponding curves display no mixing. Nevertheless, in case of the three-cluster state, see. Fig. 12(b), two points should be outlined. At variance with Fig. 12(a), not only has the difference between the dynamical correlation coefficients for the members of the same and the distinct subsets reduced but also episodes can be found where the inter-cluster correlation exceeds the intra-cluster one. This also corroborates with the statement on how the intermittent synchronization facilitates the formation of the three-cluster state: compared to the neurons in different clusters, those within the same cluster enjoy prolonged intervals of mutually coherent spiking with rare and short interruptions.

In Sec. VI, the aim is to lay out the unifying framework behind the clustering phenomena, drawing on the analysis of the common properties exhibited by the individual phase portraits. The interest lies with the microscopic mechanisms that allow the cluster states to emerge and provide for the necessary robustness against perturbations.

VI. EXPLANATION OF THE CLUSTERING DYNAMICS

Having discussed clustering from the macroscopic point of view, it is of interest to explain the way it is induced by

and how it is manifested in the behavior on a microscopic level. An improved understanding on how the dynamics of neurons participating the distinct clusters is mutually adjusted can be gained by drawing an analogy between the motion of the fast variables and that of particles in a double-well potential.³⁹ Making a change of variables $t = \epsilon t'$, one can rewrite the equations for x_i from Eq. (1) in the form $dx_i = -\frac{\partial V(x_i, y_i, X)}{\partial x_i} dt'$. The V_i potentials reduced to each of the fast subsystems then read

$$V_i(x_i, y_i, X) = -\frac{1}{2}(1-c)x_i^2 + \frac{1}{12}x_i^4 + x_i y_i - c x_i X, \quad (7)$$

incorporating both the intrinsic and the interaction terms. It is natural to treat y_i and the delayed ensemble average $X(t-\tau)$ as parameters, with the former changing at a rate much slower than x_i . One notes how the local minima and the maximum of the given V_i coincide with the intersections that the curve $y_i - cX = \text{const}$, referring to the “dressed” slow variable makes with the fast variable nullcline. The latter’s profile is, apart from the flattening effect due to interaction (the y -values at the knees are $\pm \frac{2}{3}(1-c)^{3/2}$), very much the same as that displayed in Fig. 1(a). In particular, of the three branches, the minima are tied to the refractory and the spiking ones, whereas the maximum is linked to the unstable branch. Within this framework, the spiking dynamics can be understood in terms of crossing the potential barrier between the two wells.

One may capture how the variations of the barrier’s height and the wells’ depth are reflected in the local dynamics by monitoring the simultaneous positions the arbitrary members of the distinct clusters occupy in relation to the corresponding V_i curves, see Fig. 13. The focus is on the changes in the form of the potential induced by the neurons visiting some characteristic points along the orbit. For ease of presentation, one neuron (solid V_i curves) is selected as referential, such that the Figs. 13(a)–13(c) coincide, in the respective order, with the peak of the spike, the onset of the refractory period and the resting state approaching the left knee of the slow manifold. In the first two instances, the transition barriers are expectedly high, whilst the other neuron assumes notably less stable positions on the refractory

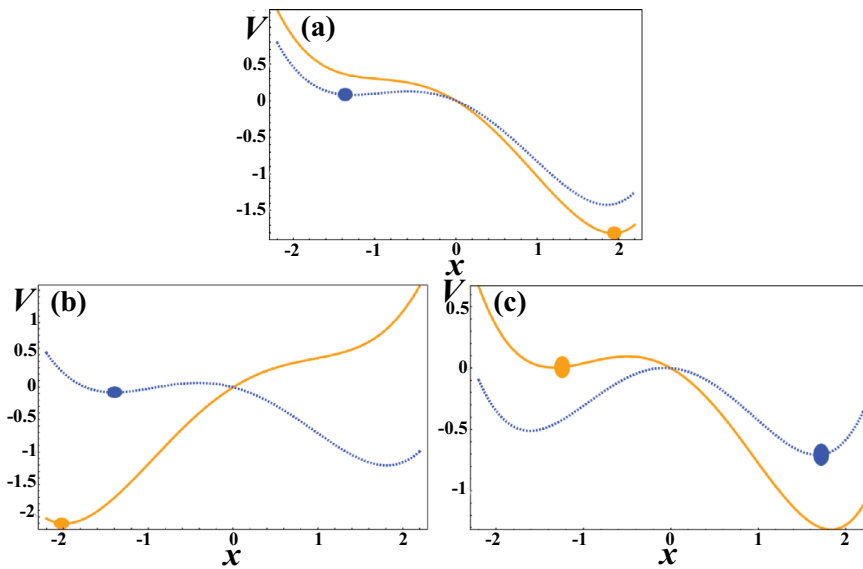


FIG. 13. Analysis of the local dynamics in analogy to motion of particles in a double-well potential. The solid and dotted curves $V_i(x_i(t), y_i(t), X(t - \tau))$ indicate the respective potentials attributed to representative neurons from the distinct clusters. Transitions between the refractory ($x \leq -1$) and the spiking ($x \geq 1$) branches are interpreted as hopping over the potential barrier, whose height depends on the interaction term. (a) reflects the setup where one neuron is active, and the other is refractory. The configuration in (b) shows both neurons on the refractory branch, with one having just completed a spike, whereas the other approaches the left knee. In (c) one of the neurons is trapped on the refractory branch, which constitutes a hallmark of clustering on the local level.

branch. Nevertheless, the most important point concerns Fig. 13(c) aimed to convey the actual signature of the clustering phenomena impressed on the local dynamics. What is demonstrated amounts to a trapping effect, where the neuron nearby, but sufficiently above the left knee, faces a very low barrier. However, its potential is almost, yet not quite enough to escape from the refractory to the spiking branch. In fact, it can be shown that the neuron is kept frustrated precisely due to the interaction term, which raises the barrier up on the value determined solely by y_i , enough to make the transition impossible. This type of behavior is maintained over the lower section of the refractory branch, with the net result of the spike generated later than the “barren” neuron dynamics would yield under the same conditions.

The discussion related to Fig. 13(c) can be appreciated by drawing a comparison between the individual phase portraits typical for neurons participating the homogeneous coherent states and the cluster states, see Figs. 14(a) and 14(b), respectively. It immediately strikes that the latter possesses a kink on the refractory branch of the slow manifold,³³ which derives from the trapping effect described above. For

the moment, we refer to the two-cluster state, a natural approach knowing the three-cluster state to be descended from it. Either way, the presence of the kink is the key manifestation of the self-regulation mechanism based on the $D - \tau$ co-effect which gives rise to the ensemble split into clusters and allows the established phase relationship among them to be maintained. The role of the kink consists in keeping the neurons frustrated on the refractory branch so to postpone the phase point’s descent toward the left knee. This scenario conforms to a lock-and-release type of behavior, where the delayed interactions primarily give rise to the former, and the action of noise to the latter part. If a fraction of neurons were to move past the left knee while the rest lagged behind, for the convenient D and τ the kink emerges to stabilize the inter-cluster separation, simultaneously strengthening the inner cluster cohesion. The location of the kink, which depends on the parameter set, is a decisive factor for the trapping effect to succeed: it has to be placed nearby the knee of the refractory branch, where the neuron dynamics is most susceptible to perturbation, yet the sufficient distance to the equilibrium has to be maintained.

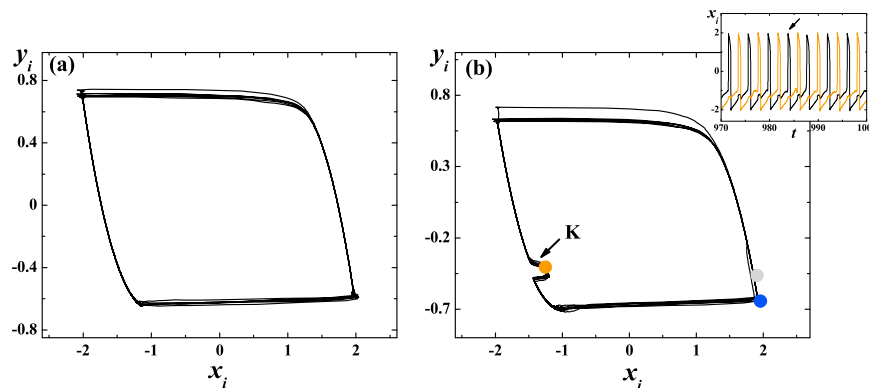


FIG. 14. (a) and (b) display the phase portraits for the local dynamics of the homogeneous coherent states and the cluster states, respectively. The latter are distinguished by the kink K , which reflects the $D - \tau$ co-effect. The inset shows sections of $x_i(t)$ series for two arbitrary members of the distinct clusters, whereby an arrow indicates the neuron, whose portrait is presented in the main frame. For an insight into the role of kink, we highlighted by bullets the respective positions of the involved neurons along the orbit at a given moment t . As a neuron lies at the kink, the other’s potential is at the peak of the rising phase (farthest right bullet). In addition, at $t - \tau$, the former is located very close to the peak, which illustrates how the delay affects the adjustment between the clusters’ dynamics. The parameters are set to $(c, D, \tau) = (0.1, 0.0005, 6)$ in (a) and $(c, D, \tau) = (0.1, 0.00025, 2)$ in (b).

The episode at the kink onset presents the sole section along the limit cycle where the interaction term prevails over the noise proper. Then, for a brief period, prompted by the rise in x_i the evolution of y_i gets accelerated to match the rate of change in the direction orthogonal to the slow manifold, the whole event driven by the spiking subset of the population. Note that the condition on the trapping interval duration is imposed as prerequisite to sustain the entrainment to a single frequency between the neurons. This frequency agrees with the one in a delay-free case, ensuring that the system dynamics takes on the form most resilient against small perturbations. Such a remark, combined with the established π phase difference for the two-cluster partition, implies that clustering may prefer some delay values over the others. One should recall here the earlier stated approximate formula for the clustering-resonant delays $\tau_r = T_0/2 + n * T_0$, where T_0 stands for the period of coherent oscillations in case of $\tau = 0$. The given expression and the subdivision of interaction terms in which the “periodical forcing” prevails over the “implicit noise” are in fact two sides of the same coin, as forcing cannot fulfill its role unless the delay is not properly adjusted so that cluster compactness can be maintained. As for the noise, the increase of τ has to be countered by the larger D to facilitate relaxation from the kink to the slow manifold while retaining the entrainment to the proper frequency. In this context, the larger noise amplitudes may begin to manifest in a wider spread of the active subset. One can see conceptually how the enhanced delays are then required to cancel, or rather average out such an effect, instating a form of control through delayed feedback.

Building on the analysis so far, we provide an additional perspective on the dynamical instability found in the three-cluster states, viz., Sec. V. Looking back at the proposed scenarios, one is seen as emerging in parallel to the kink’s occurrence, and the other is tied to its collapse. In the former case, a neuron may exchange clusters by skipping to fire within its subpopulation beat, as it sticks too long in a close proximity of the equilibrium, performing a turn around the fixed point before resettling to the original limit cycle. Within the framework involving the double-well potential, the postponed firing instability unfolds via a scenario where a delayed rise in the interaction term combined with a small y_i value effectively causes an inhibitory effect. This reestablishes the barrier in lieu of the single solution on the spiking branch, setting the neuron temporarily back in the vicinity of the potential minimum on the refractory branch.

Under the alternative scenario, the neuron firing may precipitate the rest of its cluster by virtue of the interaction terms winning over the action of noise proper. This prevents the relaxation to the refractory branch of the slow manifold, so that the neuron traverses instead a smaller orbit inside the area of phase space encircled by the typical limit cycle. The effective disappearance of the kink is tied to the collapse of the V potential barrier, the reason for it lying in that the interaction term acquires a positive value while the neuron’s phase point has not yet reached the left knee. The collapse leaves the minimum at the spiking branch as the only solution, such that getting further descent terminated promotes a smaller limit cycle orbit. To put this matter into a broader

perspective, one may recall the distinction between the CR and the SISR phenomena on non-interacting neurons, whose respective limit cycles exhibit a similar relationship.³⁹ In view of the detailed structure of the interaction terms, it may be tempting to interpret the local dynamics behind the two-cluster partition as the CR-like behavior, and the second scenario on dynamical instability as a sign of a mixed mode³⁸ where SISR-like phenomena step in.

Following the study on how the collective activity is reflected in that of individual neurons, the final section deals with the macroscopic dynamics from the perspective of the MF approximation we have derived. Two main points are introduced: first, one shows the MF model to undergo a global bifurcation for the parameter set where the exact system exhibits the onset of clustering, and second, there is further clarification on the role of noise within the D - τ interplay inducing the cluster states.

VII. THE MF MODEL AND CLUSTERING

Appreciating the all-to-all coupling scheme, one is led to develop a MF approximation to the exact model (1), an approach where the thermodynamic limit $N \rightarrow \infty$ on the population size enters in a natural way. In general, the MF treatment consists in reducing the original set of SDDE to a novel system of DDE in terms of cumulants or the moments of distribution describing deviations around the ensemble averages. In either case, the equation for the quantity of arbitrary order may involve a number of higher orders, leaving an issue of how to truncate the series that may appear unclosed.¹⁶ In this sense, the cumulant method is more convenient for it provides a plausible closure hypothesis within the Gaussian approximation, which states that the instantaneous distributions of local variables are Gaussian and that the ensemble averages at any given moment coincide with the expectation values of the appropriate distributions. If these two conditions are met, all the cumulants above second order are supposed to vanish. The detailed derivation based on these broad assumptions may be found in Ref. 28, whereas the final result reads

$$\begin{aligned} \epsilon \frac{dX(t)}{dt} &= X(t) - X(t)^3/3 - \frac{X(t)}{2} \{1 - c - X(t)^2 \\ &\quad + \sqrt{[c - 1 + X(t)^2]^2 + 4D}\} \\ &\quad - Y(t) + c[X(t - \tau) - X(t)], \\ \frac{dY(t)}{dt} &= X(t) + b. \end{aligned} \quad (8)$$

The particular form of the system (8) is a corollary of an observation exclusive to the problem at hand, which establishes the characteristic time scales of the second-order cumulants to be much longer than those of the first-order ones.

Though a simplification, the MF model should still reflect, at least qualitatively, the dynamical regimes of the exact system. The previously carried out analysis on local bifurcations displayed by the approximate system with respect to D and τ as control parameters^{28,34} has revealed a succession of supercritical and subcritical Hopf bifurcations

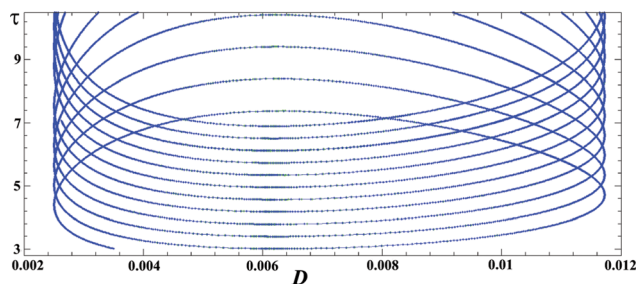


FIG. 15. Sequence of Hopf bifurcation curves for the MF model under increasing D and τ . Though the curves can account for the transitions between the stochastically stable fixed point and the stable limit cycle, one cannot associate them with the cluster formation.

under increasing delay if past the noise amplitude $D \approx 0.0025$. This is corroborated in Fig. 15 numerically by means of the DDE-biftool,^{65,66} an adaptable package of MATLAB routines suitable for handling the sets of DDE with constant delays. There is a clear interpretation on these results. The supercritical Hopf bifurcations account for the transitions between the stochastically stable fixed point and the stable limit cycle, the latter implying the existence of the parameter regions where the exact system becomes equivalent to the deterministic one. Likewise, the subcritical bifurcations suggest how introducing specific delays may put out the global coherent oscillations. Nonetheless, all the implicated noise amplitudes are $D \geq 0.0025$, too far up on the values where the cluster states are seen to kick in, which makes it legitimate to rule out any of the local bifurcations of the approximate system as linked to the phenomenon.

However, an important point we pursue is that the MF model is capable of anticipating the onset of cluster states in a range of small D , c , and τ . In particular, one finds the system (8) to undergo a global bifurcation at the parameter values around $\tau = 2$, $D = 0.00025$, $c = 0.08$. Under the given D and τ , for $c < 0.08$ there is only the equilibrium, whereas about $c \approx 0.08$ a large and a small limit cycle are born via the fold-cycle scenario. On the latter, note how the phase portrait for the MF system in Fig. 16(a) acquires the form reminiscent of the one for the exact system, viz., Fig. 5(a). The two discernable segments on the orbit are supposed to mirror the action of the subsets emerging within the actual population. This structure of the limit cycle goes unstable with increasing c and τ , in both cases suffering from the stronger impact of the interaction term. An interesting point on the MF model is that the complex-shaped limit cycle coexists with the fixed point, a behavior apparently absent in the exact system. However, mapping the respective basins of attraction in Fig. 16(b) yields that the equilibrium is nested very close to their boundary, meaning it is stochastically unstable and therefore unobservable in the exact model for an arbitrarily small noise. On the particular choice of initial function for the mean-field variables X and Y , the evolution within the time interval $t \in [-\tau, 0]$ is obtained by numerically integrating the set (8) for $c = 0$ starting off from X_0 and Y_0 . Making an analogy to the exact system, this is equivalent to assuming that all the neurons act as noninteracting elements for $t \in [-\tau, 0]$. Nonetheless, it is found that the main

result on the equilibrium lying close to the boundary between its attraction basin and that of the limit cycle, also stands for other forms of the initial function.

Though the approximate system is less likely to provide accurate predictions once D and τ are enhanced, one can still gain some insight on the nature of their coaction and its influence on the dynamics of the real system. This especially refers to setups with larger τ which admit clustering. Under these conditions, the equilibrium appears as pseudo-stable in the MF dynamics, that is the limit cycle orbits remain too long nearby the fixed point, rendering the population periods longer than in the actual model, see Fig. 16(c). Extending the last analogy, such a behavior may be interpreted as exaggerating the likelihood for the “skip to fire” events, or in other words, overestimating the possibility to observe in the real system the minor oscillations around its fixed point. The distinct phenomena due to the lack of stochastic effects in the MF approximation can in fact pose “fortunate failures,” since they might help us pinpoint the role played by the noise in the exact model. Here, it is suggested how noise may be constructive in maintaining the cluster partition by keeping the neurons from mingling outside their subsets, i.e., it is assumed to suppress the excessive cluster exchange by cutting on its leading contribution from the “skip to fire” mechanism. The two discussed instances at small and moderate D and τ demonstrate that the MF approximation can be sensitive enough to account, both qualitatively and quantitatively, for the complex phenomena in the collective dynamics of the actual model. Nevertheless, in terms of reaching an explanation, its application is not a straightforward one, with the pitfalls related to establishing the proper analogies between the behaviors the given two systems display.

VIII. SUMMARY AND DISCUSSION

We have studied the dynamics of a collection of stochastically perturbed Fitzhugh-Nagumo excitable units with time-delayed diffusive couplings. In particular, our interest has lied in analyzing the spontaneous formation of clusters, whereby the neurons within each subset are synchronized, but different clusters become active at different phases of the population oscillation. Apart from discussing the means to characterize the cluster states and their dependence on the parameter set, we have gained an insight into the dynamical mechanism responsible for clustering. In conditional terms, i.e. having fixed the excitability property of neurons, the adjustment between noise intensity and time delay is found to provide the sufficient and necessary conditions that allow for the cluster states to emerge. The latter refers to the demonstrated resonant character of the clustering effect in general, rather than making a claim on the particular set of parameter values that admit clustering. No heterogeneity in the coupling scheme or the distribution of the intrinsic neuronal parameters is required for the clusters to emerge. Nevertheless, the two-cluster partition has been verified to be robust if a small disparity of these model parameters is introduced.

Several techniques have been employed to describe and understand the synchronization clustering, starting off with

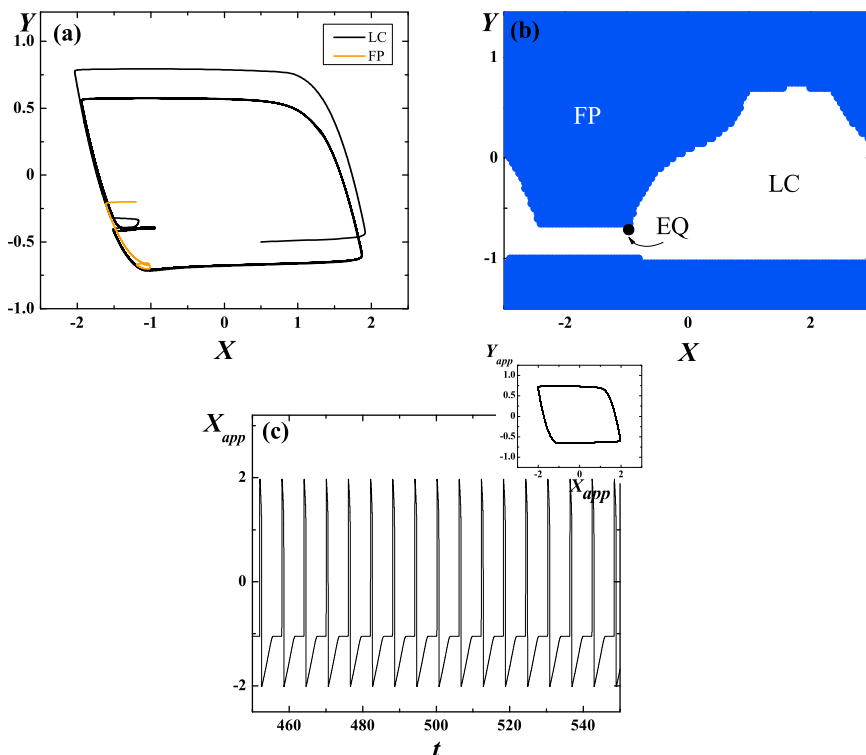


FIG. 16. Behavior of the MF model in the parameter domains related to clustering. (a) and (b) illustrate bistability observed for $D = 0.00025$, $\tau = 2$ at $c = 0.1$. (a) Shows the examples of trajectories converging either to the fixed point or the limit cycle, contingent on the initial conditions. In (b) are mapped the corresponding basins of attraction, with the equilibrium (EQ) found to lie very close to their boundary. (c) Refers to the “fortunate failure” of the approximate model under the increased D and τ . The time series and the phase portrait are provided for $(D, \tau, c) = (0.0005, 6, 0.1)$.

the methods to detect and visualize the clusters. To that end, the pairwise coherence κ_{ij} (2) was used. In fact, after applying a convenient transformation, the matrix κ_{ij} assumes a block-matrix form where the diagonal blocks mirror the clusters, and the off-diagonal blocks present the inter-cluster correlations. Two- and three-cluster distributions have been observed for different parameter values. Global coherence κ , obtained as the average of κ_{ij} , is used to study the dependence of the cluster formation on the parameters D , τ and c , viz., the noise intensity, time-lag, and the coupling strength, respectively. In order to investigate the dynamical properties of clusters, we have considered the distribution of local jitters (3), turning out to be quite useful in highlighting the differences between the dynamical properties of the two- and three-cluster regimes. The long-term behavior and the asymptotic dynamics as the population size N is increased have also been discussed. On the former, the two-cluster partition has been established as stable, whereas the internal structure of the three-cluster states has been found to involve a two-cluster nucleus and a non-negligible fraction of neurons jumping between the hard cores. The difference between the dynamical behaviors of two- and three-cluster states (stationary against the dynamical clustering) is also reflected in the dynamical correlation coefficient (6). Following on that, we turned to an explanation of the mechanism behind clustering, based on treating the evolution of the neuronal fast variables as if it referred to the motion of particles subjected to a double-well potential (7). A local manifestation of clustering is shown to be the kink formation nearby the knee of the refractory branch of the individual neuron orbit, a finding one can use to provide the qualitative explanation on the conditions necessary for the occurrence of clusters. Finally, we have demonstrated that a global fold-limit

cycle bifurcation in the approximate MF model can indicate the onset of the cluster states, further elaborating on how the proper interpretation of the reasons for some of the apparently artificial behavior displayed by the MF may serve to clarify the roles played by the particular parameters in the exact system.

Numerous recent studies have revealed formation of synchronization clusters in networks of oscillators or excitable neurons.^{10,29} However, for the most part the phenomenon is seen to arise due to the locally variable parameters, viz., Refs. 67 and 68 or as induced by the dynamically varying couplings, e.g., Ref. 69. The collection of neurons studied here is completely structureless, so that the synchronization clusters are formed by the subtle interplay of noise, interaction time-delay and the excitable nature of the units. Nevertheless, at least some of the spontaneous clustering is shown to be stable under small perturbations of the local parameters and the pattern of neuron interconnections. Such resilience may be interpreted as further indicator of possible real world applications, in particular in the context of facilitating the neural encoding or improving its capacity. Most prominently, this refers to cognitive processes of binding and segmentation. In the former instance, multiple representations of the same object may be bound into a cluster state, whereas in the latter, clustering is supposed to contribute in discriminating between the distinct perceptual entities.^{29,70} At variance with the beneficial roles, certain pathological brain rhythms linked to the epileptic seizures involve a high frequency firing of neural populations that might emerge through the interspersed action of several clusters.¹⁰ On the formal side, it would be interesting to investigate whether the spontaneous synchronization clustering also occurs in networks of excitable systems with a different types of excitability.

ACKNOWLEDGMENTS

This work was supported in part by the Ministry of Education and Science of the Republic of Serbia, under Project Nos. 171017 and 171015.

- ¹L. M. Ward, *Trends Cogn. Sci.* **17**, 553 (2003).
- ²O. Jensen, J. Kaiser, and J.-P. Lachaux, *Trends Neurosci.* **30**, 317 (2007).
- ³A. K. Engel, P. Fries, and W. Singer, *Nat. Rev. Neurosci.* **2**, 704 (2001).
- ⁴F. Varela *et al.*, *Nat. Rev. Neurosci.* **2**, 229 (2001).
- ⁵G. Buzsáki and A. Draguhn, *Science* **304**, 1926 (2004).
- ⁶S. N. Baker *et al.*, *Exp. Brain Res.* **128**, 109 (1999).
- ⁷M. Cassidy *et al.*, *Brain* **125**, 1235 (2002).
- ⁸J. N. Sanes and J. P. Donoghue, *Proc. Natl. Acad. Sci. U.S.A.* **90**, 4470 (1993).
- ⁹V. N. Murthy and E. E. Fetz, *J. Neurophysiol.* **76**, 3949 (1996).
- ¹⁰*Coordinated Activity in the Brain: Measurements and Relevance to Brain Function and Behavior*, edited by J. L. P. Velazquez and R. Wennberg (Springer, New York, 2009).
- ¹¹M. D. McDonnell and L. M. Ward, *Nat. Rev. Neurosci.* **12**, 415 (2011).
- ¹²*Coherent Behavior in Neuronal Networks* edited by K. Josić, J. Rubin, M. A. Matías, and R. Romo (Springer, New York, 2009).
- ¹³C. E. Smith, in *Single Neuron Computation*, edited by T. McKenna, J. Davis, and S. F. Zorntzer (Academic, San Diego, CA, 1992).
- ¹⁴A. Longtin, *Phys. Rev. E* **55**, 868 (1997).
- ¹⁵E. Manjarrez *et al.*, *Neurosci. Lett.* **326**, 93 (2002).
- ¹⁶B. Lindner, J. Garcia-Ojalvo, A. Neiman, and L. Schimansky-Geier, *Phys. Rep.* **392**, 321 (2004).
- ¹⁷E. V. Pankratova, A. V. Polovinkin, and B. Spagnolo, *Phys. Lett. A* **344**, 43 (2005).
- ¹⁸D. Valenti, G. Augello, and B. Spagnolo, *Eur. Phys. J. B* **65**, 443 (2008).
- ¹⁹A. S. Pikovsky and J. Kurths, *Phys. Rev. Lett.* **78**, 775 (1997).
- ²⁰H. D. I. Abarbanel *et al.*, *Neural Comput.* **8**, 1567 (1996).
- ²¹M. Dhamala, V. K. Jirsa, and M. Ding, *Phys. Rev. Lett.* **92**, 074104 (2004).
- ²²N. Burić and D. Todorović, *Phys. Rev. E* **67**, 066222 (2003).
- ²³E. Rossoni, Y. Chen, M. Ding, and J. Feng, *Phys. Rev. E* **71**, 061904 (2005).
- ²⁴D. V. Ramana Reddy, A. Sen, and G. L. Johnson, *Phys. Rev. Lett.* **80**, 5109 (1998).
- ²⁵S. H. Strogatz, *Nature (London)* **394**, 316 (1998).
- ²⁶O. V. Popovych, C. Hauptmann, and P. A. Tass, *Phys. Rev. Lett.* **94**, 164102 (2005).
- ²⁷G. Buzsáki, *Rhythms of the Brain* (Oxford University Press, Oxford, 2006).
- ²⁸N. Burić, K. Todorović, and N. Vasović, *Physica A* **389**, 3956 (2010).
- ²⁹P. A. Tass, *Phase Resetting in Medicine and Biology: Stochastic Modeling and Data Analysis* (Springer, Berlin/Heidelberg, 2007).
- ³⁰D. Golomb and J. Rinzel, *Physica D* **72**, 259 (1994).
- ³¹K. Okuda, *Physica D* **63**, 424 (1993).
- ³²U. Ernst, K. Pawelzik, and T. Geisel, *Phys. Rev. E* **57**, 2150 (1998).
- ³³I. Franović, K. Todorović, N. Vasović, and N. Burić, *Phys. Rev. Lett.* **108**, 094101 (2012).
- ³⁴N. Burić, K. Todorović, and N. Vasović, *Phys. Rev. E* **82**, 037201 (2010).
- ³⁵E. M. Izhikevich, *Dynamical Systems in Neuroscience: The Geometry of Excitability and Bursting* (MIT, Cambridge, Massachusetts, 2007).
- ³⁶*Complex Time-Delay Systems: Theory and Applications*, edited by F. M. Atay (Springer, Berlin/Heidelberg, 2010).
- ³⁷E. Scholl, G. Hiller, P. Hovel, and M. A. Dahlem, *Philos. Trans. R. Soc. London, Ser. A* **367**, 1079 (2009).
- ³⁸C. B. Muratov and E. Vanden-Eijnden, *Chaos* **18**, 015111 (2008).
- ³⁹R. E. Lee DeVillie, E. Vanden-Eijnden, and C. B. Muratov, *Phys. Rev. E* **72**, 031105 (2005).
- ⁴⁰C. B. Muratov, E. Vanden-Eijnden, and E. Weinan, *Physica D* **210**, 227 (2005).
- ⁴¹P. Kaluza, C. Strege, and H. Meyer-Ortmanns, *Phys. Rev. E* **82**, 036104 (2010).
- ⁴²H. Hasegawa, *Physica D* **237**, 137 (2008).
- ⁴³J. A. Acebrón, A. R. Bulsara, and W.-J. Rappel, *Phys. Rev. E* **69**, 026202 (2004).
- ⁴⁴H. Hasegawa, *Phys. Rev. E* **67**, 041903 (2003).
- ⁴⁵M. A. Zaks, A. B. Neiman, S. Feistel, and L. Schimansky-Geier, *Phys. Rev. E* **68**, 066206 (2003).
- ⁴⁶Y. Gao and J. Wang, *Phys. Rev. E* **83**, 031909 (2011).
- ⁴⁷S. Luccioli and A. Politi, *Phys. Rev. Lett.* **105**, 158104 (2010).
- ⁴⁸S. Olmi, A. Politi, and A. Torcini, *EPL* **92**, 60007 (2010).
- ⁴⁹M. Rosenblum and A. Pikovsky, *Phys. Rev. E* **70**, 041904 (2004).
- ⁵⁰M. Rosenblum and A. Pikovsky, *Phys. Rev. Lett.* **92**, 114102 (2004).
- ⁵¹M. Yi and L. Yang, *Phys. Rev. E* **81**, 061924 (2010).
- ⁵²X. Sun, M. Perc, Q. Lu, and J. Kurths, *Chaos* **20**, 033116 (2010).
- ⁵³O. Sporns, *Networks of the Brain* (MIT, Cambridge, 2011).
- ⁵⁴E. Bullmore and O. Sporns, *Nat. Rev. Neurosci.* **10**, 186 (2009).
- ⁵⁵O. Sporns, D. Chialvo, M. Kaiser, and C. C. Hilgetag, *Trends Cogn. Sci.* **8**, 418425 (2004).
- ⁵⁶V. M. Eguluz *et al.*, *Phys. Rev. Lett.* **94**, 018102 (2005).
- ⁵⁷P. Fries, *Trends Cogn. Sci.* **9**, 474 (2005).
- ⁵⁸M. K. S. Yeung and S. H. Strogatz, *Phys. Rev. Lett.* **82**, 648 (1999).
- ⁵⁹G. Schmid, I. Goychuk, and P. Hnggi, *Physica A* **325**, 165 (2003).
- ⁶⁰G. B. Ermentrout and D. H. Terman, *Mathematical Foundations of Neuroscience* (Springer, New York, 2010).
- ⁶¹D. T. W. Chik, S. Coombes, and Z. D. Wang, *Phys. Rev. E* **70**, 011908 (2004).
- ⁶²X. Sailer *et al.*, *Phys. Rev. E* **73**, 056209 (2006).
- ⁶³D. Golomb, D. Hansel, and G. Mato, in *Neuro-Informatics and Neural Modelling*, edited by F. Moss and S. Gielen (Elsevier, Amsterdam, 2000).
- ⁶⁴I. Franović and V. Miljković, *Chaos, Solitons Fractals* **44**, 122 (2011).
- ⁶⁵K. Engelborghs, T. Luzyanina, and G. Samaey, Technical Report No. TW-330, Department of Computer Science, K. U. Leuven, Leuven, Belgium, 2001.
- ⁶⁶K. Engelborghs, T. Luzyanina, and D. Roose, *ACM Trans. Math. Softw.* **28**, 1 (2002).
- ⁶⁷V. K. Jirsa, *Cognit. Neurodynamics.* **2**, 29 (2008)
- ⁶⁸M. Li, S. Guan, and C.-H. Lai, *New J. Phys.* **12**, 103032 (2010).
- ⁶⁹R. K. Niyogi and L. Q. English, *Phys. Rev. E* **80**, 066213 (2009).
- ⁷⁰W. Singer and C. M. Gray, *Annu. Rev. Neurosci.* **18**, 555 (1995).

Chaos is copyrighted by the American Institute of Physics (AIP). Redistribution of journal material is subject to the AIP online journal license and/or AIP copyright. For more information, see <http://ojps.aip.org/chaos/chocr.jsp>